



Spray Coating Experiments: Setups and Methodologies



**The latest eBook from
Advanced Optical Metrology.
Download for free.**

Spray Coating Experiments: Setups and Methodologies, is the third in our Thin Films eBook series. This publication provides an introduction to spray coating, three article digests from Wiley Online Library and the latest news about Evident's Image of the Year Award 2022.

Wiley in collaboration with Evident, are committed to bridging the gap between fundamental research and industrial applications in the field of optical metrology. We strive to do this by collecting and organizing existing information, making it more accessible and useful for researchers and practitioners alike.

EVIDENT
OLYMPUS

WILEY

J-Type Self-Assembled Supramolecular Polymers for High-Performance and Fast-Response n-Type Organic Electrochemical Transistors

Kai-Kai Liu, Peiyun Li, Yuqiu Lei, Zhuoqiong Zhang, Xiran Pan, Shu Kong So, and Ting Lei*

To date, high-performance organic electrochemical transistors (OECTs) are almost all based on conjugated polymers. Small molecules can be synthesized with high purity without batch-to-batch variations. However, small molecules require highly crystalline films and good molecular packings to achieve high charge carrier mobilities. Such features make their films unsuitable for ion diffusion or make their molecular packing distorted due to ion diffusion, resulting in poor ion/charge carrier transport properties and slow response speed. Herein, it is proposed to construct small-molecule-based supramolecular polymers to address these issues. A molecule, namely TDPP-RD-G7 is designed, which exhibits J-type self-assembling behaviors and can form supramolecular polymers in solution and conjugated-polymer-like networks in solid state. More importantly, the porous supramolecular polymer networks allow fast ion diffusion and greatly increase the device response speeds. As a result, the TDPP-RD-G7 exhibits record fast response speeds ($\tau_{\text{on}}/\tau_{\text{off}}$) of 10.5/0.32 ms with high figure-of-merit (μC^*) of $5.88 \text{ F cm}^{-1} \text{ V}^{-1} \text{ s}^{-1}$ in small-molecule OECTs. This work reveals the possible reasons that hinder the response speeds in small-molecule OECTs and demonstrates a new “supramolecular polymer” approach to high-performance and fast-response small-molecule-based OECTs.

high transconductance, and good bio-compatibility. OECTs have been widely used in transducing and amplifying low-amplitude electrophysiological signals, metabolite sensors, and neuromorphic computing.^[1–3] To evaluate the performance of an OECT material, two important parameters are often used: 1) the intrinsic capability of transducing voltage signals to current signals, known as a figure-of-merit, μC^* ; 2) on/off switching speeds ($\tau_{\text{on}}/\tau_{\text{off}}$) of an OECT device. The OECT steady-state performance (μC^*) can be evaluated using the following equation (Equation 1):

$$g_m = \frac{\partial I_D}{\partial V_G} = \frac{W}{L} \cdot d \cdot \mu \cdot C^* \cdot (V_{\text{Th}} - V_G) \quad (1)$$

where μ is the electronic charge carrier mobility, C^* is the volumetric capacitance, W , d , and L are the channel width, depth, and length, respectively; V_{Th} is the threshold voltage, and V_G is the gate voltage. As shown in Equation 1, the g_m

depends on both material's figure-of-merit (μC^*) and device geometry-dependent terms (Wd/L). The response speeds are also important, especially for applications, such as real-time signal amplification, high-quality bio-interfacing transmission, and neuromorphic computing.^[4,5] Recent years have witnessed the fast development of OECT materials. P-type OECT polymers have shown high device performances ($\mu\text{C}^* > 200 \text{ F cm}^{-1} \text{ V}^{-1} \text{ s}^{-1}$) and fast on/off response speeds ($\tau_{\text{on}} < 1 \text{ ms}$; $\tau_{\text{off}} < 0.1 \text{ ms}$).^[6–13] Although n-type conjugated polymers lag behind,^[14–25] recent works have demonstrated high μC^* over $50 \text{ F cm}^{-1} \text{ V}^{-1} \text{ s}^{-1}$ and comparable on/off response speeds ($\tau_{\text{on}} < 2 \text{ ms}$; $\tau_{\text{off}} < 0.2 \text{ ms}$).^[26–29] Based on p- and n-type OECT materials, both high-performance complementary logic circuits and neuron-like electronics have been demonstrated.^[25,29,30] However, to date, almost all high-performance OECT materials are based on conjugated polymers.^[6,11,12,31–37]


Small molecules have precise chemical structures, no batch-to-batch variations, better device stability, and usually higher charge carrier mobilities.^[38,39] Because of these features, more and more efforts have been devoted to exploring small-molecule OECT materials.^[40–46] Ginger et al. chose fullerenes as the building block and reported fullerene derivatives with

1. Introduction

Organic electrochemical transistors (OECTs) have attracted increasing attention due to their low operating voltage ($< 1 \text{ V}$),

K.-K. Liu, P. Li, X. Pan, T. Lei
Key Laboratory of Polymer Chemistry and Physics of Ministry of Education
School of Materials Science and Engineering
Peking University
Beijing 100871, China
E-mail: tinglei@pku.edu.cn

Y. Lei
College of Engineering
Peking University
Beijing 100871, China
Z. Zhang, S. K. So
Department of Physics
Institute of Advanced Materials
Hong Kong Baptist University
Kowloon Tong SAR 224, Hong Kong

 The ORCID identification number(s) for the author(s) of this article can be found under <https://doi.org/10.1002/adfm.202300049>.

DOI: 10.1002/adfm.202300049

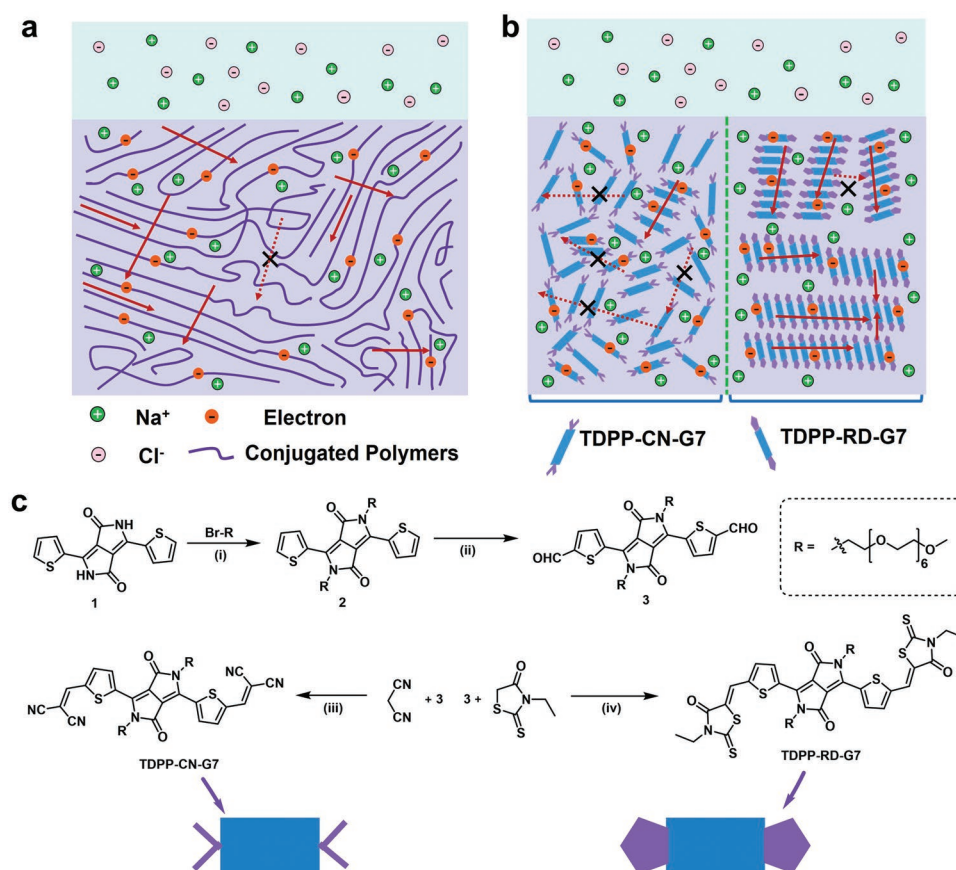


Figure 1. Challenges for small-molecule OECT material design and our “supramolecular polymer” approach. a) The “tie-chain” networks in conjugated polymers. Ions can diffuse into films without damaging charge transport pathways. b) Illustration of the ion diffusion in small molecules with weak intermolecular interactions (e.g., TDPP-CN-G7) and strong interactions (e.g., TDPP-RD-G7). The red solid arrows represent efficient charge transport pathways; the red dashed arrows with black cross represent inefficient charge transfer pathways. Sodium ions, chloride ions, and electrons (negative polarons) on backbones are shown with green, light pink, and orange circles, respectively. c) Synthetic approaches to the small molecules, TDPP-CN-G7, and TDPP-RD-G7. Reagents and conditions: i) K_2CO_3 , DMF, 110 °C, 12 h, 70%; ii) a. LDA, THF, -78 °C, 1 h, b. -78 °C to 50 °C, DMF, 1 h, 25%; iii) EtOH, CHCl_3 , β -Alanine, 25 °C, 24 h, 55%; iv) Et_3N , CHCl_3 , reflux, 5 h, 65%.

ethylene glycol (EG) side chains (C60-TEG), which shows a high μC^* value of $7 \text{ F cm}^{-1} \text{ V}^{-1} \text{ s}^{-1}$ with no response time data.^[40] Yue et al. introduced rigid multi-component fused-ring to enhance the OECT performance, leading to good solid-state molecular packing and improved μC^* of $10.3 \text{ F cm}^{-1} \text{ V}^{-1} \text{ s}^{-1}$ and response speeds ($\tau_{\text{on}}/\tau_{\text{off}}$) of 439/84 ms. However, both the fullerene derivatives and fused ring skeletons are complicated with long synthetic steps and high costs. In addition, to date, almost all small-molecule OECTs showed slow response speeds (Table S4, Supporting Information). We hypothesize that the large fullerenes and fused rings are too hydrophobic with close molecular packings, which might inhibit ions' fast diffusion/penetration, resulting in slower response speeds.

The fast response feature of polymers may originate from their “tie-chain” networks, which allow fast ion diffusions while keeping good charge transport properties (Figure 1a).^[29] However, small molecules do not possess these characteristics.^[47] During device operation, the infiltrated ions will destroy ordered molecular packing and significantly reduce the charge carrier mobility (μ), resulting in low μC^* (Figure 1b).^[41] Therefore, how to develop a simple and more

general strategy to achieve high device performance and make small molecules tolerant to ion penetrations/diffusions are still challenging. Here, for the first time, we propose to construct supramolecular polymers to overcome the above issues, making small molecules more tolerant to ion diffusions like traditional conjugated polymers (Figure 1b). Two small molecules, TDPP-CN-G7 and TDPP-RD-G7, were synthesized for comparison. We combined absorption/fluorescence spectra, in situ dynamic spectroscopy, dynamic light scattering (DLS), single crystal structure analysis, theoretical calculations, and morphology characterization etc., to observe and analyze the self-assembly behaviors of the molecules and demonstrated that small molecules that can form supramolecular polymers might be potential candidates for high-performance and fast-response OECTs. TDPP-RD-G7 can form J-type supramolecular polymers in solution and a microscopic “conjugated-polymer-like” network in film. These features lead to good charge transport pathways and efficient ion penetration/diffusion. As a result, a high OECT figure-of-merit (μC^*) of $5.88 \text{ F cm}^{-1} \text{ V}^{-1} \text{ s}^{-1}$ and record fast response speeds ($\tau_{\text{on}}/\tau_{\text{off}}$) of 10.5/0.32 ms are achieved.

2. Results and Discussion

2.1. Design, Synthesis, and Characterization

Thiophene-flanked diketopyrrolopyrrole (TDPP) was chosen as the building block because it has a large π -conjugated plane with strong intermolecular interactions and can be readily functionalized.^[48] We introduced two different electron-deficient functional groups, malononitrile (CN) and 3-ethylrhodanine (RD) as the functional groups to tune the molecular lowest unoccupied molecular orbital (LUMO) energy levels and their intermolecular interactions (Figure 1c). Hydrophilic oligo (ethylene glycol) (EG) side chains were used to ensure good solubility and hydrophilicity. Two small molecules, TDPP-CN-G7 and TDPP-RD-G7, were obtained. We assumed that the larger end-capping group RD might provide stronger intermolecular interactions (Figure 1b).

Figure 1c illustrates the synthetic routes to both molecules and their structure characterizations are detailed in the Supporting Information. Two oligo ethylene glycol (G7) chains were installed onto TDPP under basic conditions, yielding compound 2. Compound 2 was then lithiated by Lithium diisopropylamide (LDA) in tetrahydrofuran solution at $-78\text{ }^{\circ}\text{C}$ and subsequently quenched by dry dimethylformamide (DMF) at $50\text{ }^{\circ}\text{C}$ to afford compound 3. Compound 3 was subjected to Knoevenagel condensation reaction with CN or RD, giving TDPP-CN-G7 and TDPP-RD-G7, respectively.^[49] Both molecules showed excellent thermal stability with decomposition temperatures over $320\text{ }^{\circ}\text{C}$ (Figure S1, Supporting Information). Differential scanning calorimetry (DSC) measurement shows that both molecules have two major phase transitions. The melting points for TDPP-CN-G7 and TDPP-RD-G7 are $110\text{--}130$ and $195\text{--}208\text{ }^{\circ}\text{C}$, respectively (Figure S1, Supporting Information). The higher melting point of TDPP-RD-G7 suggests that it might have stronger intermolecular interactions.

Density functional theory (DFT) calculations show that both molecules have a planar configuration. The calculated highest occupied molecular orbital (HOMO)/LUMO energy levels of TDPP-CN-G7 and TDPP-RD-G7 are $-6.09\text{--}4.28$ and $-5.57\text{--}3.78\text{ eV}$.^[48] The HOMO/LUMO energy levels of TDPP-CN-G7 and TDPP-RD-G7 measured by cyclic voltammetry (CV) are $-5.76\text{ eV}/-4.26$ and $-5.55\text{ eV}/-4.05\text{ eV}$, consistent with the DFT calculation results (Figure S2 and Table S1, Supporting Information). The low LUMO energy levels suggest that the two small molecules could show n-type charge transport behaviors.

2.2. Formation of J-Type Supramolecular Polymers

Both molecules show two absorption bands in solution: Band I from 400 to 500 nm ; Band II from 550 to 700 nm (Figure 2a,b). In the film, a new absorption peak at a longer wavelength appears for both molecules, suggesting that they form strong solid-state interactions with certain kinds of aggregates. However, the aggregates of two molecules show distinct absorption peaks. The peak of TDPP-CN-G7 shows comparable absorption intensity as its original Band II peaks, whereas TDPP-RD-G7 shows much-increased intensity with significantly decreased Band II peaks. In addition, TDPP-RD-G7 has a small Stokes

shift (42 nm) compared to TDPP-CN-G7 (50 nm) in solution, and in film, the Stokes shift of TDPP-RD-G7 becomes even smaller (10.5 nm) whereas that of TDPP-CN-G7 becomes larger (81 nm), suggesting that TDPP-RD-G7 has a more rigid backbone and more ordered aggregation than TDPP-CN-G7 in solid state. Furthermore, the fluorescent intensity of TDPP-CN-G7 did not change much before and after annealing. However, the fluorescent intensity of TDPP-RD-G7 enhanced after annealing (Figure S3, Supporting Information). According to previous theoretical and experimental studies, all these features can be attributed to the formation of J-type aggregation in solid state for TDPP-RD-G7.^[50,51]

To dynamically probe the solution-state aggregation behavior of the two small molecules in solution, we measured the spectrum changes of the two molecules by adding poor solvent *n*-hexane into their tetrachloroethane (TCE) solutions. As shown in Figure 2c,d, the aggregation peaks start to appear above $n\text{-hexane}/\text{TCE} = 80/20$, suggesting both molecules start to aggregate at this ratio. These results also indicate that the J-type aggregates are formed in solution. To confirm that the J-type aggregates can also form during spin-coating or solvent evaporation process, we adopted the in situ dynamic spectroscopy (DS) method to characterize the dynamic absorption spectra of two small molecules from solution to film and then to annealed film.^[52] As is shown in Figure 2e,f, the absorption spectra of both TDPP-CN-G7 and TDPP-RD-G7 were gradually changing during spin-coating ($1\text{--}300\text{ s}$). After annealing ($300\text{--}900\text{ s}$), the aggregates' absorption peaks of TDPP-CN-G7 were almost unchanged, but those of TDPP-RD-G7 were further enhanced (Figure S4, Supporting Information). These results indicate that the J-type aggregates are formed in solution and can be deposited onto a substrate. Thermal annealing can also enhance the molecular packing order in solid state.

Dynamic light scattering (DLS) was further used to verify the formation of J-type aggregated supramolecular polymers in solution. DLS analysis could provide the aggregates' size during adding hexane to TCE (Figure 2g–j). DLS measurement shows that the particle size is $\approx 1\text{ nm}$ and the small molecule is in a monodispersed state ($n\text{-hexane}/\text{TCE} = 0/100$). When the small molecules start to aggregate ($n\text{-hexane}/\text{TCE} > 80/20$), new aggregates with size $\approx 200\text{ nm}$ are formed. As the ratio increases to $85/15$, the monodispersed molecules disappear and only the 200 nm sized particles exist. At higher $n\text{-hexane}/\text{TCE}$ ratio ($>90/10$), the 200 nm aggregates start to further aggregate into 700 nm sized aggregates. Similar supramolecular polymerization and nucleation-growth process have also been observed in other types of supramolecular polymers.^[53] Therefore, we propose that the increase in the molecular size (from 1 to 200 nm) implies the formation of self-assembled J-type supramolecular polymers, and the further growth of J-aggregates (from 200 to 700 nm) may originate from the “oriented attachment” process of the supramolecular polymers.^[53]

To further verify that TDPP-RD-G7 can self-assemble into supramolecular polymers through J-type aggregation, the monodispersed solution (0.5 g L^{-1} TCE) and the solution containing aggregates (cyclohexane/TCE = $90/10$, 0.5 g L^{-1}) were spun onto a substrate rapidly to avoid further aggregation. These aggregates are probed by an atomic force microscope (AFM). AFM height images of the monodispersed solution

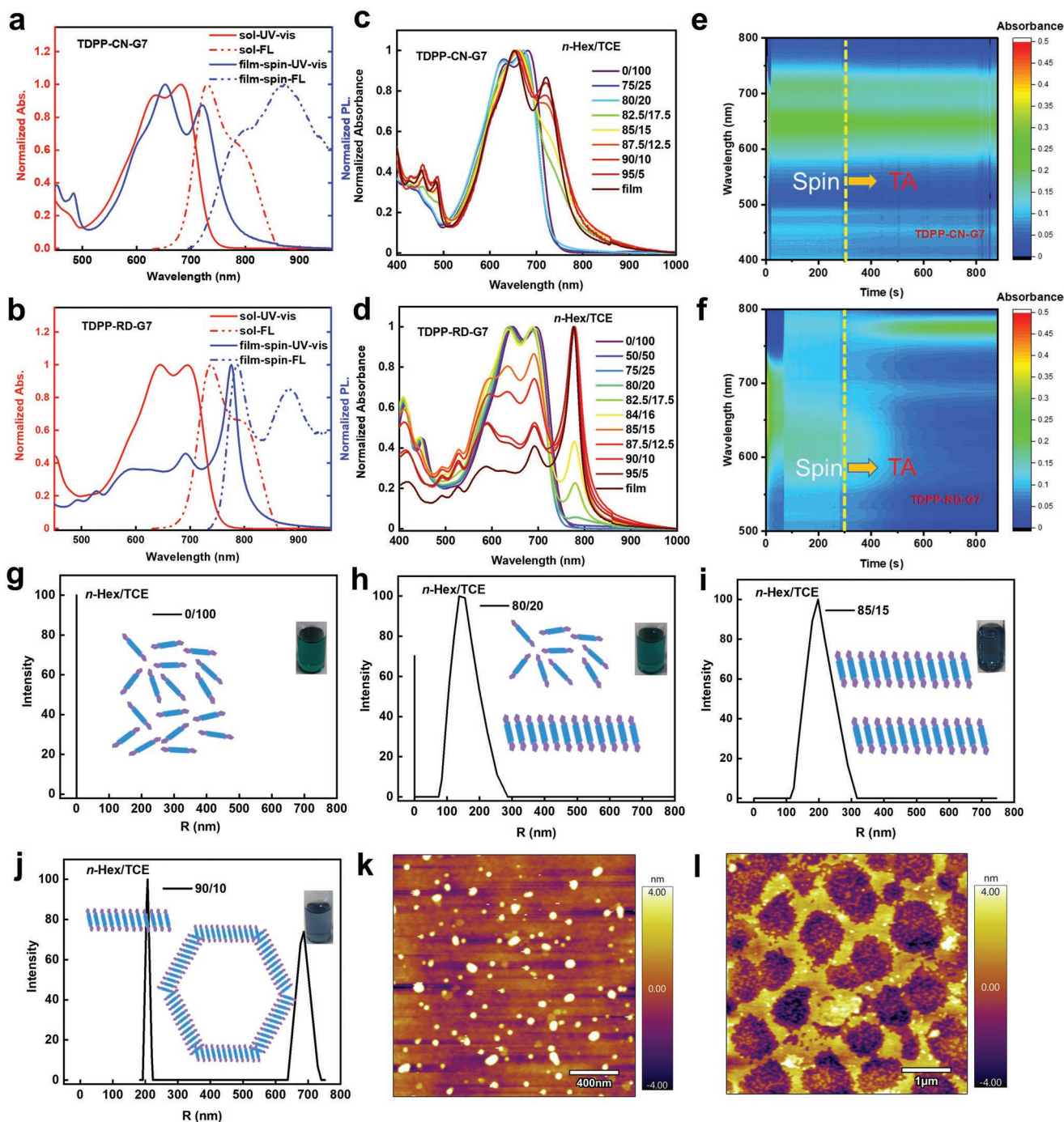


Figure 2. Formation of small-molecule-based J-type supramolecular polymers. a) Normalized absorption (solid lines) and photoluminescence (dash lines) spectra of TDPP-CN-G7 ($\lambda_{\text{ex}} = 610$ nm for red dashed lines, $\lambda_{\text{ex}} = 650$ nm for blue dashed lines) and b) TDPP-RD-G7 ($\lambda_{\text{ex}} = 610$ nm for red dashed lines, $\lambda_{\text{ex}} = 584$ nm for blue dashed line) in $\text{C}_2\text{H}_2\text{Cl}_4$ (TCE, 1.0×10^{-5} mol L^{-1}) and film. Solvent-dependent UV-vis-NIR absorption spectra of c) TDPP-CN-G7 and d) TDPP-RD-G7 in solution (*n*-hexane/TCE volume ratio). In-situ dynamic spectra from solution to the spin-coated and annealed film of e) TDPP-CN-G7 and f) TDPP-RD-G7. g–j) Dynamic light scattering (DLS) size distributions of TDPP-CN-G7 aggregates in mixed solvents with different *n*-hexane/TCE volumetric ratios (concentration: 2×10^{-5} mol L^{-1}), g) *n*-hexane/TCE = 0/100, h) *n*-hexane/TCE = 80/20, i) *n*-hexane/TCE = 85/15, j) *n*-hexane/TCE = 90/10. AFM height images of TDPP-RD-G7 film, k) coated with a 0.5 g L^{-1} TCE solution, l) coated with a 0.5 g L^{-1} mixed solution (cyclohexene/TCE = 90/10).

show several nanometer-sized particles, whereas the images of the aggregated solution show continuous fiber-like network textures (Figure 2l). These results agree well with DLS experiment

that “conjugated-polymer-like” supramolecular assemblies are formed in solution, and these supramolecular polymers can further assemble into a thin film.

2.3. Formation of Conjugated-Polymer-Like Networks by Supramolecular Polymers

To accurately illustrate the molecular packing of the supramolecular polymers formed in solution, single crystal analysis and DFT calculations were performed. The growth of the single crystals of TDPP-CN-G7 and TDPP-RD-G7 is not successful because of their poor crystallinity after introducing EG side chains. Instead, TDPP-CN-C12 and TDPP-RD-C4C6 with the same conjugated backbone but alkyl side chains were synthesized. Both alkylated molecules, TDPP-CN-C12 and TDPP-RD-C4C6 showed strong aggregation peaks in film. However, the aggregates' peaks are not as strong as TDPP-RD-G7, indicating that the molecular packing is also affected by the choice of side chains (Figure S6, Supporting Information). Both molecules exhibit a "cis" double bond conformation same as the DFT-optimized structures (Figure S2, Supporting Information). The torsional angle between the TDPP and the RD groups is 8.41°, smaller than that of the TDPP and CN (10.54°), suggesting TDPP-RD has better planarity. Both molecules show similar π - π stacking distances of 3.34 Å (TDDP-RD) and 3.36 Å (TDPP-CN) (Figure S7, Supporting Information).

Both molecules show column packing with different dislocations via π - π stacking interactions, and the dislocation might be affected by the choice of side chains (Figure S7, Supporting Information). To compare the intermolecular interactions between RD and CN, we performed DFT structural optimization using different starting packing structures (Figure S8, Supporting Information). All the starting structures are converged to a single molecular packing, suggesting the optimized packing structure is stable. TDPP-RD shows an association energy (E_a) of 204.1 kJ mol⁻¹, larger than that of 131.7 kJ mol⁻¹ for TDPP-CN. We also calculated the effect of TDPP-RD intermolecular displacement on its absorption spectra through time-dependent density functional theory (TDDFT). We found that the most stable state of intermolecular packing showed strongly red-shifted spectra, suggesting that the J-type aggregation is probably a thermodynamically stable molecular packing (Figure S9, Supporting Information). These results further confirm that TDPP-RD has stronger intermolecular interactions than TDPP-CN. Furthermore, intercolumn interactions also exist in the single crystal (Figure 3c), indicating that the J-type supramolecular polymers formed via π - π stacking can also further assemble into larger assemblies through the intercolumn interactions. These computational results well support the DLS and AFM results and analysis (Figure 2l).

To accurately illustrate the molecular packing of the supramolecular polymers formed in film, we calculated the single molecule size of TDPP-RD-G7. TDPP-RD-G7 is \approx 5.4 nm along the side chain and 2.5 nm along the backbone direction (Figure 3a). We measured the network film thickness of TDPP-RD-G7 fibers using AFM and found that the thickness of the fiber region is 5.5 nm, and the assemblies in the middle of the mesh are 2.2 nm. Thus, we propose that the self-assembled network observed in Figure 2l is a monolayer of the supramolecular polymers. The 5.5 nm thickness corresponds to a side-chain edge-on molecular packing, whereas the 2.2 nm thickness might correspond to the end group edge-on packing. The side-chain edge-on molecular packing is

consistent with the GIWAXS results (Figure 6). We also calculated that in the TDPP-RD single crystal, the intracolumn E_a is 137.6 kJ mol⁻¹, much higher than the intercolumn interaction E_a of 36.5 kJ mol⁻¹ (Figure 3c). This result further supports that TDPP-RD-G7 can self-assemble into 1D supramolecular polymers through π - π stacking interactions and then form networks through intercolumn interactions.

As shown in Figure 4a,b, we have realized J-type supramolecular self-assembly of TDPP-RD-G7 both in solution and in solid state. Based on all the above results, we propose that the self-assembly process of TDPP-RD-G7 to a mesh-like network might contain four steps (Figure 4c): 1) some of the monodispersed small molecules (2 nm) form 1D J-type supramolecular polymers (\approx 200 nm) (Figure 2g,h); 2) all the small molecules form supramolecular polymers after adding more poor solvent and during solvent evaporation; 3) 1D supramolecular polymers form larger aggregates (\approx 700) through an "oriented-attachment" process; 4) the larger aggregates are deposited on substrate to form a hexagonal mesh-like network. The reason for the preferential formation of the hexagonal structure is unclear. However, many studies have demonstrated that the hexagon packing is preferentially formed due to its lowest surface energy among different shapes,^[54] and the formation of the hexagonal network has been widely observed both in nature (e.g., bubble and honeycomb) and in the surface-tension-driven self-assembly process of functional materials.^[55]

2.4. Electrochemical Properties and OECT Device Performance

The electrochemical activity of the two small molecules was studied by spectroelectrochemistry (Figure S10a,b, Supporting Information). The changes in absorption spectra were monitored after applying different potentials in 0.1 M NaCl aqueous solution. After increasing the bias voltage from 0 to -0.5 V or 0 to -0.7 V, both TDPP-CN-G7 and TDPP-RD-G7 exhibited gradually increased polaron absorption bands (800–1200 nm). Notably, the absorption spectrum changes of TDPP-RD-G7 at 800 and 1200 nm are not obvious until the applied bias exceeds -0.5 V, higher than that of TDPP-CN-G7 (-0.3 V), which is due to the lower LUMO level of TDPP-CN-G7.

Electrochemical stability is essential for OECT devices. Continuous cyclic voltammetry (CV) scans and electrochemical spectroscopy measurements (Figure S11, Supporting Information) show that the capacitance of the TDPP-CN-G7 film attenuated significantly in the second cycle, and the reduction current continued to decrease with the increase of cycles. In contrast, the CV curves of the TDPP-RD-G7 film did not obviously decay after cycling, indicating that TDPP-RD-G7 film has better electrochemical stability. Moreover, we measured the spectrum changes after every cycle. The spectra of TDPP-CN-G7 changed greatly after the first cycle, whereas the spectra of TDPP-RD-G7 did not change. All the results prove that TDPP-RD-G7 film possesses better electrochemical doping and cycling stability, which could be attributed to its strong intermolecular interactions.

The OECT devices were fabricated by spin coating the molecules' TCE solution onto a source-drain electrode patterned substrate, and the films were then thermally annealed

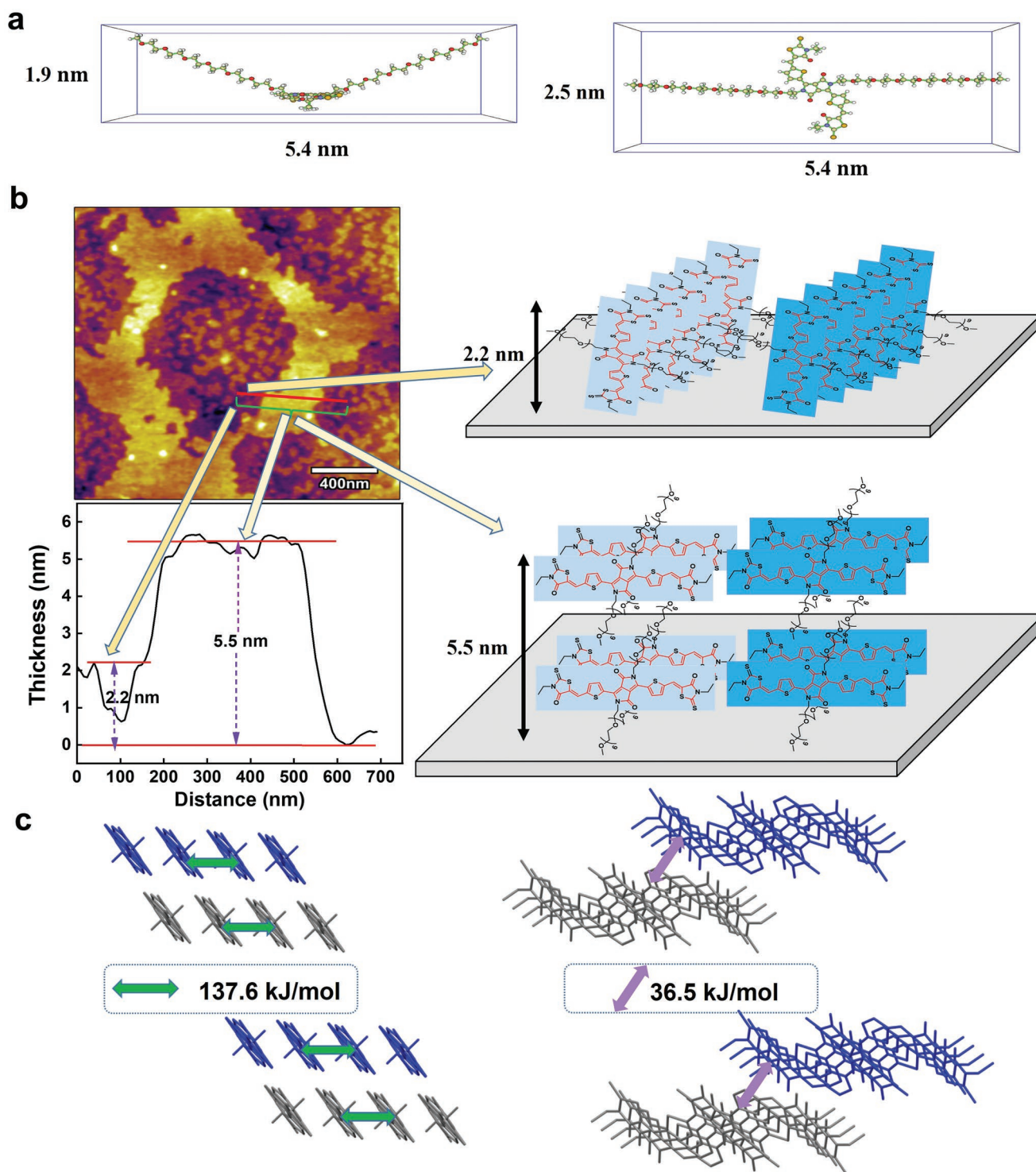


Figure 3. Understanding self-assembly of molecular monolayers. a) Single molecule size of the optimized TDPP-RD-G7 structure. b) The thickness of the fiber network film measured by AFM for TDPP-RD-G7 and different packing modes in the film. c) Single crystal molecular packing of TDPP-RD-G7 with alkyl side chains. Hydrogen atoms and side chains are omitted for clarity. Calculated association energies of the intracolumn molecular packing E_a (137.6 kJ mol⁻¹) and the intercolumn E_a (36.5 kJ mol⁻¹). Thus, the molecule tends to grow in a one-dimensional manner.

at 80 °C for 10 min. (see Supporting Information for more details). The OECT device performance is evaluated using the Bernards' model (Equation 1).^[56] Both molecules exhibit

typical n-type OECT behaviors (Figure 5 and Table 1; Table S3 and Figure S13, Supporting Information). The TDPP-CN-G7-based OECT device showed a μC^* value of 0.80 F cm⁻¹ V⁻¹ s⁻¹.

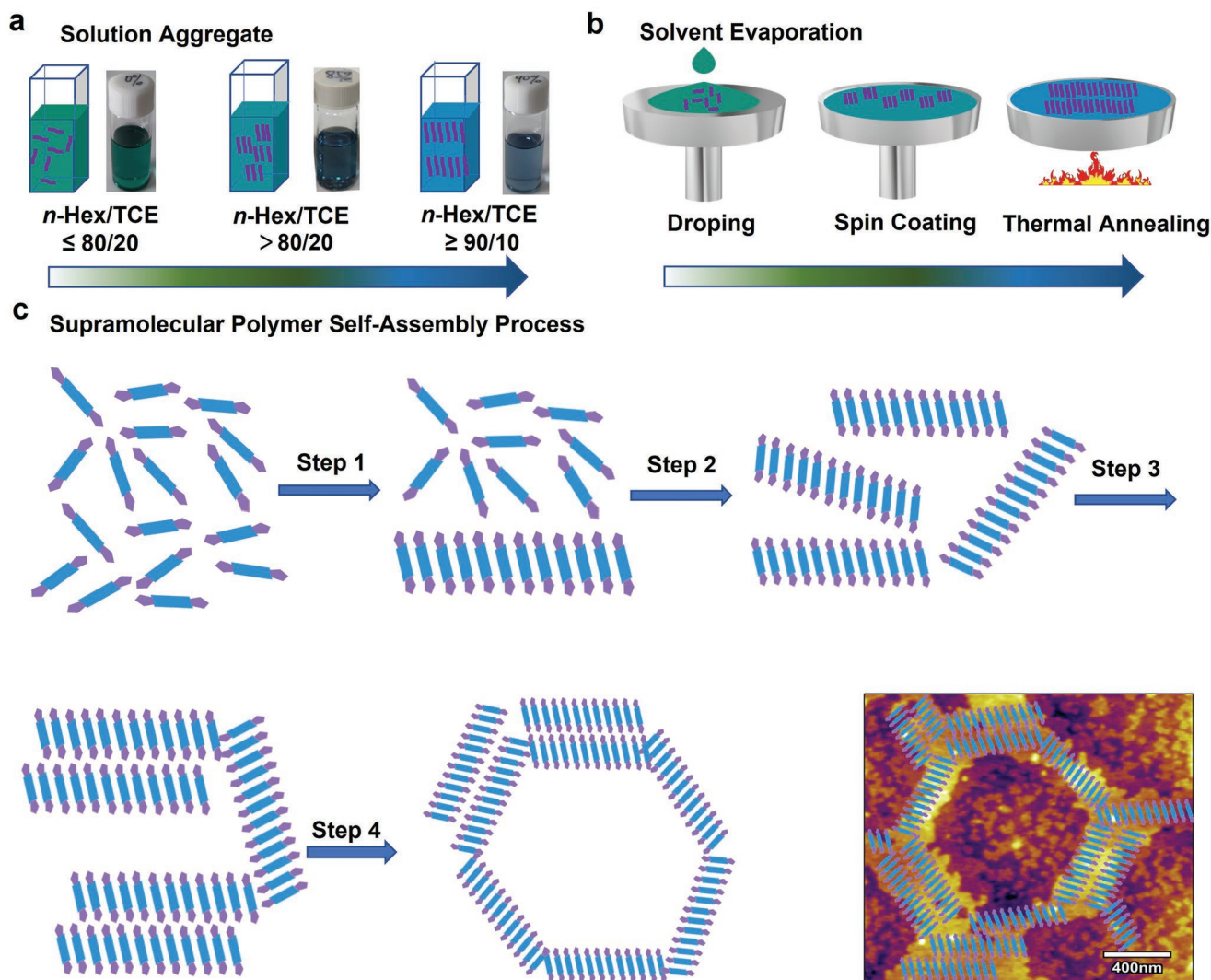


Figure 4. Understanding of the self-assembly process of TDPP-RD-G7. a) Supramolecular self-assembly in solution. b) Supramolecular self-assembly during spin-coating. c) Schematic illustration of the multi-level self-assembly process of TDPP-RD-G7.

In contrast, the TDPP-RD-G7-based device exhibited high μC^* of $5.88 \text{ F cm}^{-1} \text{ V}^{-1} \text{ s}^{-1}$, which outperforms many n-type conjugated polymers reported in literature (Figure S13b, Supporting Information).^[44–46] To further understand the performance differences between the two molecules, the volume capacitance (C^*) was measured by electrochemical impedance spectroscopy (EIS, Figure S14a,b, Supporting Information). The average value of C^* was 165.2 F cm^{-3} for TDPP-CN-G7 and 78.6 F cm^{-3} for TDPP-RD-G7. The calculated electron mobility was $0.005 \text{ cm}^2 \text{ V}^{-1} \text{ s}^{-1}$ for TDPP-CN-G7 and $0.075 \text{ cm}^2 \text{ V}^{-1} \text{ s}^{-1}$ for TDPP-RD-G7. Therefore, the higher OECT performance of TDPP-RD-G7 originates from its high charge carrier mobilities, which compensate for its relatively low volumetric capacitance. In addition, TDPP-RD-G7 exhibited good stability with over $\approx 70\%$ current retention after 100 cycles in air, much better than that of TDPP-CN-G7 ($\approx 20\%$ after 40 cycles) (Figure S15a,b, Supporting Information). To evaluate the response speed of these two small molecules, we tested the transient properties of their

OECT devices (Figure 5e; Figure S16, Supporting Information), by applying a pulse of 100 ms to the gate electrode and a DC voltage of 0.6 V to the drain electrode. Response times were estimated by the exponential fitting of the I_{DS} . TDPP-CN-G7 showed a poor response, which might be due to its disordered crystallization and poor electrical performance. TDPP-RD-G7 exhibited short response times with τ_{on} of 10.5 ms and τ_{off} of 0.32 ms, which are the fastest among all small-molecule-based OECT materials (Figure 5f; Table S4, Supporting Information). The fast speed response time may be due to the “tie-chain” network structure of TDPP-RD-G7 supramolecular polymer to accommodate ion doping more efficiently. High mobility and fast response characteristics make TDPP-RD-G7 a promising material for high-speed real-time bio-sensing applications.^[5]

To further verify the electron transport capability of both small molecules, a top-gate/bottom-contact (TG/BC) OFET device configuration was used. The active layer was deposited by spin coating the molecules' TCE solution onto an Au

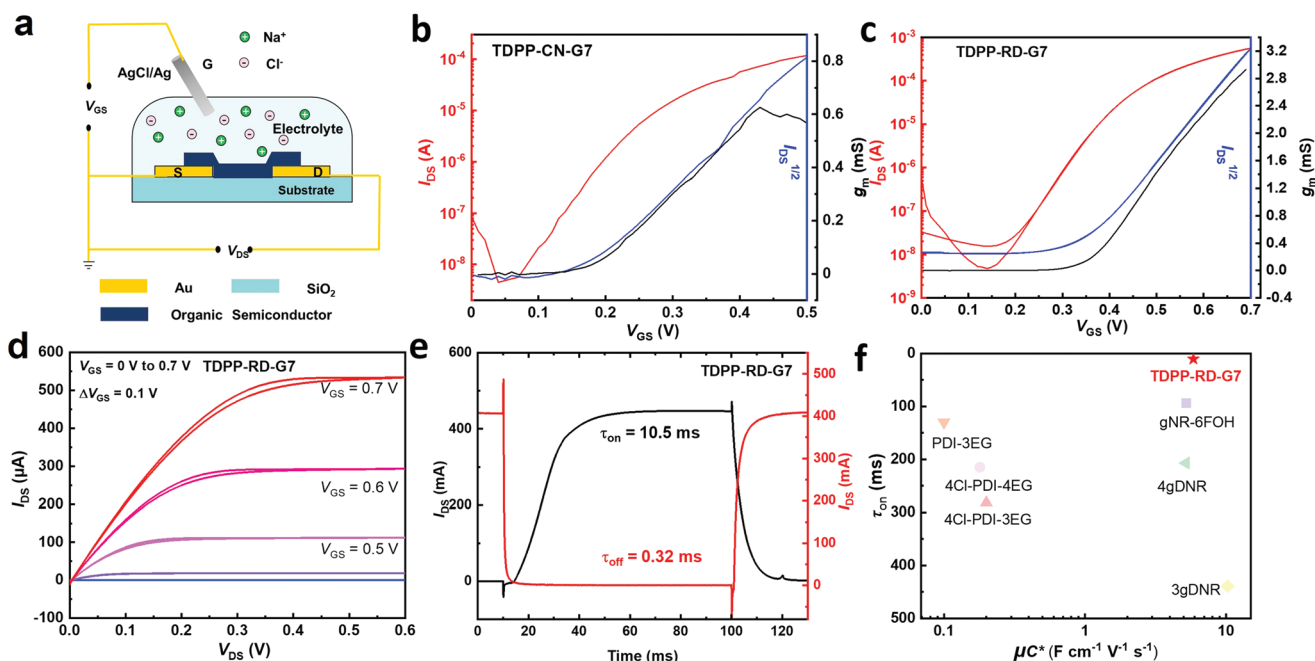


Figure 5. OECT device characterization. a) Device configuration of the OECT devices. b,c) Transfer characteristics of TDPP-CN-G7 and TDPP-RD-G7 with V_{GS} of 0–0.5 and 0–0.7 V, $V_{DS} = 0.6$ V. The black lines are the curves of g_m . The OECT devices were measured in a 0.1 M NaCl aqueous solution and the gate electrode is AgCl/Ag pellet. d) Output characteristics of a TDPP-RD-G7 OECT device. e) Transient on/off response curves with V_{GS} of 0–0.7 V for TDPP-RD-G7. f) Comparison of the τ_{on} and μC^* values of TDPP-RD-G7 with other reported small-molecule OECT materials.^[40,42–46]

(source-drain)/SiO₂/Si substrate, and the films were then thermally annealed at 80 °C for 10 min. Both small molecules show typical n-type transport characteristics under ambient conditions (Table 1; Figure S17a–d, Supporting Information) The maximum electron mobility of the TDPP-RD-G7 devices was determined to be 0.052 cm² V^{−1} s^{−1}, higher than that of TDPP-CN-G7 (0.002 cm² V^{−1} s^{−1}). Note that these values agree well with the mobility obtained from the OECT devices, demonstrating that the difference in the performance of the two molecules might originate from their different molecular packing.

The Urbach energy (E_u) is often used to evaluate the energetic disorder of an organic semiconductor film (Figure S18, Supporting Information).^[57] According to the photothermal deflection spectroscopy (PDS) measurement, the film of TDPP-RD-G7 showed an Urbach energy of 45.0 meV, slightly smaller than that of TDPP-CN-G7 (46.8 meV). Such a small Urbach energy difference could not explain the significant charge carrier mobility difference between the two molecules. Therefore, we propose that the electron mobility difference is not due to the energetic disorders of the molecules themselves, but originates from their different molecular packings.

2.5. Understanding of the Importance of Supramolecular Self-Assembly for OECTs

AFM was used to study the morphology change after doping (Figure S12, Supporting Information). In the pristine film, TDPP-CN-G7 showed a polycrystalline and rough surface, with a large root-mean-square (RMS) roughness of 9.3 nm in AFM height images. When the film was immersed in 0.1 M

NaCl aqueous electrolyte, the surface RMS of TDPP-CN-G7 decreased significantly, and the film morphology obviously changed. After CV scanning, the RMS of TDPP-CN-G7 film was further reduced, indicating that the film morphology was not stable enough. However, the TDPP-RD-G7 film has a smooth surface and small fiber-like textures with a smaller RMS of 2.6 nm. After electrochemical doping, it only showed slight swelling, without obvious change, indicating that TDPP-RD-G7 film has good ion permeability and morphology stability. Grazing incidence wide-angle X-ray scattering (GIWAXS) was used to explore the microstructure difference between two molecules. Figure 6 compares their pristine, annealed films, exposed films, and reduced films., TDPP-CN-G7 showed typical small-molecule polycrystalline diffraction patterns, which have been often observed in other small molecules with similar chemical structures.^[58] However, the TDPP-RD-G7 presents conjugated-polymer-like diffractions with an “edge-on” molecular packing, consistent with AFM measurement result in Figure 3. The conjugated-polymer-like “lamellar” (31.1 Å) and “ π - π scattering” (3.50 Å) diffractions can be observed in the out-of-plane (OOP) and in-plane (IP) directions (d_{lamellar} and $d_{\pi-\pi}$) in the pristine film, respectively (Figure 6 and Table 1; Table S5, Supporting Information). After being annealed at 80 °C for 10 min, TDPP-RD-G7 showed an increase in the coherence length in the lamellar direction ($L_{c,\text{lam}}$), and a slight decrease in the coherence length in the π - π stacking direction ($L_{c,\pi-\pi}$). After being exposed to 0.1 M NaCl aqueous solution and reduction, the diffraction peaks of TDPP-RD-G7 showed no obvious change. In contrast, after being exposed to 0.1 M NaCl aqueous solution and reduced, TDPP-CN-G7 film showed broader peaks and new peaks in the OOP direction appeared

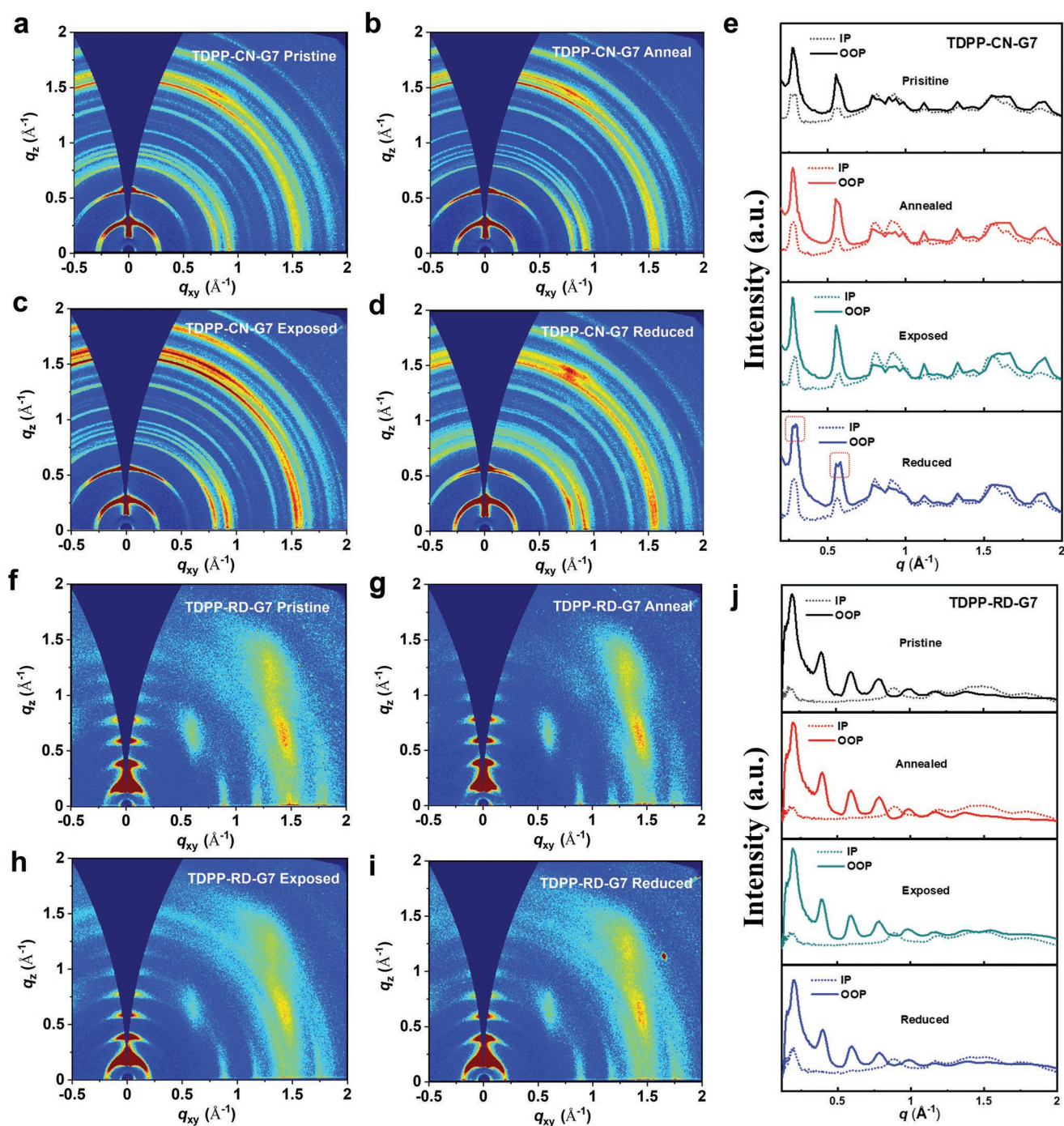


Figure 6. Molecular packing analysis of both molecules. 2D GIWAXS patterns and corresponding line-cuts for TDPP-CN-G7 and TDPP-RD-G7 of a,f) spin-coated pristine films, b,g) annealed films, c,h) exposed films, and d,i) reduced films. e,j) Line-cuts profiles from the 2D GIWAXS patterns. IP stands for in plane and OOP stands for out of plane.

(as indicated by the dashed squares in Figure 6e), suggesting that molecular packing changed significantly after reduction. These results demonstrate that the molecular packing of TDPP-RD-G7 in film shows good tolerance to ion injection/diffusion, whereas the molecular packing of TDPP-CN-G7 changed after electrochemically doping, which could explain the much better electrochemically cycling stability of TDPP-RD-G7. Therefore,

we propose that the stronger intermolecular interactions endow TDPP-RD-G7 with J-type supramolecular self-assembly behavior and a “conjugated-polymer-like” network. Such a “conjugated-polymer-like” network makes TDPP-RD-G7 behave like traditional conjugated polymers that can tolerate fast ion injection/diffusion, leading to better OECT device performance, response behaviors, and operation stability.

Table 1. Summary of the OECT/OFET Performance and Molecular Packing Parameters.

	$g_{mmax}^a)$ [mS]	$V_{th}^b)$ [V]	$\mu C^*_{max}^c)$ [F cm ⁻¹ V s]	C^* [F cm ⁻³]	τ_{on}/τ_{off} [ms]	$\mu_{OECT\ max}^d)$ [cm ² V ⁻¹ s]	$\mu_{OFET\ max}^e)$ [cm ² V ⁻¹ s]	$d_{lamellar}^f)$ [Å]	$d_{\pi-\pi}^f)$ [Å]
TDPP-CN-G7	0.31	0.16	0.80 (0.68 ± 0.11)	165.2 ± 16.1	NA	0.005	0.002	NA	NA
TDPP-RD-G7	3.5	0.34	5.88 (5.43 ± 0.37)	78.6 ± 7.5	10.5/0.32	0.075	0.052	31.1	3.50

^{a)}The W/L of all the devices is 34 000/20 μm. All the OECT devices were operated in a 0.1 M NaCl aqueous solution; ^{b)} V_{th} was determined by extrapolating the corresponding $I_{DS}^{1/2}$ versus V_{GS} plots; ^{c)}Three devices were tested and computed for each small molecule. μC^* was calculated according to Equation (1); ^{d)} μ_{OECT} was calculated from the μC^* and the measured volumetric capacitance C^* ; ^{e)}Electron mobilities are measured under ambient conditions; ^{f)} $d_{lamellar}$ and $d_{\pi-\pi}$ stacking distances were determined by GIWAXS experiments. NA stands for not available.

3. Conclusion

In summary, we first propose a supramolecular polymer approach to address the poor device performance, slow response, and stability issues for small-molecule-based OECTs. We found that TDPP-RD-G7 with a J-type aggregation behavior endows the molecule with a “conjugated-polymer-like” network film. The network could benefit fast ion injection/diffusion and enables the TDPP-RD-G7 film to exhibit high n-type OECT performance with a figure-of-merit (μC^*) of 5.88 F cm⁻¹ V⁻¹ s⁻¹ and record fast response speeds (τ_{on}/τ_{off}) of 10.5/0.32 ms in small-molecule OECTs. Our work demonstrates that constructing supramolecular polymers is a good approach to address the poor ion penetration/diffusion issues and slow response behaviors of small-molecule OECTs.

Supporting Information

Supporting Information is available from the Wiley Online Library or from the author.

Acknowledgements

This work was supported by National Natural Science Foundation of China (92156019 and 22075001), Beijing Natural Science Foundation (JQ22006), and National Key Research and Development Project (2022YFE0130600). K.-K.L. thanks the China Postdoctoral Science Foundation (2021M690196) and the Boya Postdoctoral Fellowship of Peking University. The authors acknowledge the Molecular Materials and Nanofabrication Laboratory (MMNL) in the College of Chemistry and Electron Microscopy Laboratory of Peking University for the use of instruments. The computational part is supported by High-Performance Computing Platform of Peking University. The authors thank Dr. Liang Li and Prof. Huanping Zhou from Peking University for their help in dynamic spectroscopy (DS). The authors thank Dr. Guangqi Wu and Prof. Hua Lu from Peking University for their help in dynamic light scattering (DLS).

Conflict of Interest

The authors declare no conflict of interest.

Author Contributions

K.-K.L. and P.L. contributed equally to this work. K.-K.L. and X.P. synthesized the small molecules and performed some characterization.

P.L. performed device fabrication and characterization. Y.L. performed DFT calculations. Z.Z. and S.K.S. performed the PDS measurement. K.-K.L., P.L., and T.L. wrote the manuscript. All the authors revised and approved the manuscript.

Data Availability Statement

The data that support the findings of this study are available from the corresponding author upon reasonable request.

Keywords

J-type self-assembly, organic electrochemical transistors, small molecules, supramolecular polymers

Received: January 3, 2023

Revised: January 30, 2023

Published online:

- [1] N. A. Kukhta, A. Marks, C. K. Luscombe, *Chem. Rev.* **2022**, *122*, 4325.
- [2] J. Rivnay, S. Inal, A. Salleo, R. M. Owens, M. Berggren, G. G. Malliaras, *Nat. Rev. Mater.* **2018**, *3*, 17086.
- [3] Y. van de Burgt, E. Lubberman, E. J. Fuller, S. T. Keene, G. C. Faria, S. Agarwal, M. J. Marinella, A. Alec Talin, A. Salleo, *Nat. Mater.* **2017**, *16*, 414.
- [4] J. Rivnay, P. Leleux, M. Ferro, M. Sessolo, A. Williamson, D. A. Koutsouras, D. Khodagholy, M. Ramuz, X. Strakosas, R. M. Owens, C. Benar, J.-M. Badier, C. Bernard, G. G. Malliaras, *Sci. Adv.* **2015**, *1*, e1400251.
- [5] C. Cea, G. D. Spyropoulos, P. Jastrzebska-Perfect, J. J. Ferrero, J. N. Gelinas, D. Khodagholy, *Nat. Mater.* **2020**, *19*, 679.
- [6] R. K. Hallani, B. D. Paulsen, A. J. Petty, R. Sheelamanthula, M. Moser, K. J. Thorley, W. Sohn, R. B. Rashid, A. Savva, S. Moro, J. P. Parker, O. Drury, M. Alsufyani, M. Neophytou, J. Kosco, S. Inal, G. Costantini, J. Rivnay, I. McCulloch, *J. Am. Chem. Soc.* **2021**, *143*, 11007.
- [7] L. Huang, Z. Wang, J. Chen, B. Wang, Y. Chen, W. Huang, L. Chi, T. J. Marks, A. Facchetti, *Adv. Mater.* **2021**, *33*, 2007041.
- [8] L. Lan, J. Chen, Y. Wang, P. Li, Y. Yu, G. Zhu, Z. Li, T. Lei, W. Yue, I. McCulloch, *Chem. Mater.* **2022**, *34*, 1666.
- [9] X. Luo, H. Shen, K. Perera, D. T. Tran, B. W. Boudouris, J. Mei, *ACS Macro Lett.* **2021**, *10*, 1061.
- [10] M. Moser, A. Savva, K. Thorley, B. D. Paulsen, T. C. Hidalgo, D. Ohayon, H. Chen, A. Giovannitti, A. Marks, N. Gasparini, A. Wadsworth, J. Rivnay, S. Inal, I. McCulloch, *Angew. Chem. Int. Ed.* **2021**, *60*, 7777.

- [11] J. L. Rivnay, Pierre, M. Ferro, M. Sessolo, A. Williamson, D. A. Koutsouras, D. Khodagholy, M. Ramuz, X. Strakosas, R. M. Owens, C. Benar, J.-M. Badier, C. Bernard, G. G. Malliaras, *Sci. Adv.* **2015**, *1*, e1400251.
- [12] A. Giovannitti, D. T. Sbircea, S. Inal, C. B. Nielsen, E. Bandiello, D. A. Hanifi, M. Sessolo, G. G. Malliaras, I. McCulloch, J. Rivnay, *Proc. Natl. Acad. Sci. USA* **2016**, *113*, 12017.
- [13] H. Jia, Z. Huang, P. Li, S. Zhang, Y. Wang, J.-Y. Wang, X. Gu, T. Lei, *J. Mater. Chem. C* **2021**, *9*, 4927.
- [14] X. Chen, A. Marks, B. D. Paulsen, R. Wu, R. B. Rashid, H. Chen, M. Alsufyani, J. Rivnay, I. McCulloch, *Angew. Chem. Int. Ed.* **2021**, *60*, 9368.
- [15] A. Giovannitti, C. B. Nielsen, D. T. Sbircea, S. Inal, M. Donahue, M. R. Niazi, D. A. Hanifi, A. Amassian, G. G. Malliaras, J. Rivnay, I. McCulloch, *Nat. Commun.* **2016**, *7*, 13066.
- [16] I. P. Maria, B. D. Paulsen, A. Savva, D. Ohayon, R. Wu, R. Hallani, A. Basu, W. Du, T. D. Anthopoulos, S. Inal, J. Rivnay, I. McCulloch, A. Giovannitti, *Adv. Funct. Mater.* **2021**, *31*, 2008718.
- [17] A. Marks, X. Chen, R. Wu, R. B. Rashid, W. Jin, B. D. Paulsen, M. Moser, X. Ji, S. Griggs, D. Meli, X. Wu, H. Bristow, J. Strzalka, N. Gasparini, G. Costantini, S. Fabiano, J. Rivnay, I. McCulloch, *J. Am. Chem. Soc.* **2022**, *144*, 4642.
- [18] Z. S. Parr, J. Borges-Gonzalez, R. B. Rashid, K. J. Thorley, D. Meli, B. D. Paulsen, J. Strzalka, J. Rivnay, C. B. Nielsen, *Adv. Mater.* **2022**, *34*, 2107829.
- [19] A. F. Paterson, H. Faber, A. Savva, G. Nikiforidis, M. Gedda, T. C. Hidalgo, X. Chen, I. McCulloch, T. D. Anthopoulos, S. Inal, *Adv. Mater.* **2019**, *31*, 1902291.
- [20] R. B. Rashid, A. M. Evans, L. A. Hall, R. R. Dasari, E. K. Roesner, S. R. Marder, D. M. D'Allesandro, W. R. Dichtel, J. Rivnay, *Adv. Mater.* **2022**, *34*, 2110703.
- [21] J. Shi, P. Li, X.-Y. Deng, J. Xu, Z. Huang, Y. Lei, Y. Wang, J.-Y. Wang, X. Gu, T. Lei, *Chem. Mater.* **2022**, *34*, 864.
- [22] H. Sun, M. Vagin, S. Wang, X. Crispin, R. Forchheimer, M. Berggren, S. Fabiano, *Adv. Mater.* **2018**, *30*, 1704916.
- [23] J. Surgailis, A. Savva, V. Druet, B. D. Paulsen, R. Wu, A. Hamidi-Sakr, D. Ohayon, G. Nikiforidis, X. Chen, I. McCulloch, J. Rivnay, S. Inal, *Adv. Funct. Mater.* **2021**, *31*, 2010165.
- [24] Y. Wang, E. Zeglio, L. Wang, S. Cong, G. Zhu, H. Liao, J. Duan, Y. Zhou, Z. Li, D. Mawad, A. Herland, W. Yue, I. McCulloch, *Adv. Funct. Mater.* **2022**, *32*, 2111439.
- [25] C. Y. Yang, M. A. Stoeckel, T. P. Ruoko, H. Y. Wu, X. Liu, N. B. Kolhe, Z. Wu, Y. Puttison, C. Musumeci, M. Massetti, H. Sun, K. Xu, D. Tu, W. M. Chen, H. Y. Woo, M. Fahlman, S. A. Jenekhe, M. Berggren, S. Fabiano, *Nat. Commun.* **2021**, *12*, 2354.
- [26] K. Feng, W. Shan, S. Ma, Z. Wu, J. Chen, H. Guo, B. Liu, J. Wang, B. Li, H. Y. Woo, S. Fabiano, W. Huang, X. Guo, *Angew. Chem. Int. Ed.* **2021**, *60*, 24198.
- [27] K. Feng, W. Shan, J. Wang, J. W. Lee, W. Yang, W. Wu, Y. Wang, B. J. Kim, X. Guo, H. Guo, *Adv. Mater.* **2022**, *34*, 2201340.
- [28] H. Y. Wu, C. Y. Yang, Q. Li, N. B. Kolhe, X. Strakosas, M. A. Stoeckel, Z. Wu, W. Jin, M. Savvakis, R. Kroon, D. Tu, H. Y. Woo, M. Berggren, S. A. Jenekhe, S. Fabiano, *Adv. Mater.* **2022**, *34*, 2106235.
- [29] P. Li, J. Shi, Y. Lei, Z. Huang, T. Lei, *Nat. Commun.* **2022**, *13*, 5970.
- [30] P. C. Harikesh, C. Y. Yang, D. Tu, J. Y. Gerasimov, A. M. Dar, A. Armada-Moreira, M. Massetti, R. Kroon, D. Bliman, R. Olsson, E. Stavrinidou, M. Berggren, S. Fabiano, *Nat Commun* **2022**, *13*, 901.
- [31] B. Ding, G. Kim, Y. Kim, F. D. Eisner, E. Gutierrez-Fernandez, J. Martin, M. H. Yoon, M. Heeney, *Angew. Chem. Int. Ed.* **2021**, *60*, 19679.
- [32] S. Inal, G. G. Malliaras, J. Rivnay, *Nat. Commun.* **2017**, *8*, 1767.
- [33] H. J. Kim, K. Perera, Z. Liang, B. Bowen, J. Mei, B. W. Boudouris, *ACS Macro Lett* **2022**, *11*, 243.
- [34] J. H. Kim, S. M. Kim, G. Kim, M. H. Yoon, *Macromol Biosci* **2020**, *20*, 2000211.
- [35] A. T. Lill, D. X. Cao, M. Schrock, J. Vollbrecht, J. Huang, T. Nguyen-Dang, V. V. Brus, B. Yurash, D. Leifert, G. C. Bazan, T. Q. Nguyen, *Adv. Mater.* **2020**, *32*, 1908120.
- [36] M. Moser, L. R. Savagian, A. Savva, M. Matta, J. F. Ponder, T. C. Hidalgo, D. Ohayon, R. Hallani, M. Reijjalali, A. Troisi, A. Wadsworth, J. R. Reynolds, S. Inal, I. McCulloch, *Chem. Mater.* **2020**, *32*, 6618.
- [37] C. B. Nielsen, A. Giovannitti, D. T. Sbircea, E. Bandiello, M. R. Niazi, D. A. Hanifi, M. Sessolo, A. Amassian, G. G. Malliaras, J. Rivnay, I. McCulloch, *J. Am. Chem. Soc.* **2016**, *138*, 10252.
- [38] J. Chen, W. Zhang, L. Wang, G. Yu, *Adv. Mater.* **2023**, <https://doi.org/10.1002/adma.202210772>.
- [39] W. Jiang, Z. Liu, D. Zhu, W. Zheng, L. Chen, X. Zhang, G. Zhang, Y. Yi, L. Jiang, D. Zhang, *Angew. Chem. Int. Ed.* **2021**, *60*, 10700.
- [40] C. G. Bischak, L. Q. Flagg, K. Yan, C. Z. Li, D. S. Ginger, *ACS Appl. Mater. Interfaces* **2019**, *11*, 28138.
- [41] J. Duan, G. Zhu, L. Wang, J. Chen, S. Cong, X. Zhu, Y. Zhou, Z. Li, I. McCulloch, W. Yue, *Adv. Funct. Mater.* **2022**, *32*, 2203937.
- [42] H. Liao, J. Chen, L. Lan, Y. Yu, G. Zhu, J. Duan, X. Zhu, H. Dai, M. Xiao, Z. Li, W. Yue, I. McCulloch, *ACS Appl. Mater. Interfaces* **2022**, *14*, 16477.
- [43] Z. S. Parr, R. B. Rashid, B. D. Paulsen, B. Poggi, E. Tan, M. Freeley, M. Palma, I. Abrahams, J. Rivnay, C. B. Nielsen, *Adv. Electron. Mater.* **2020**, *6*, 2000215.
- [44] J. Duan, G. Zhu, L. Lan, J. Chen, X. Zhu, C. Chen, Y. Yu, H. Liao, Z. Li, I. McCulloch, W. Yue, *Angew. Chem. Int. Ed.* **2022**, *62*, e202213737.
- [45] E. Stein, O. Nahor, M. Stolov, V. Freger, I. M. Petruta, I. McCulloch, G. L. Frey, *Nat. Commun.* **2022**, *13*, 5548.
- [46] G. Zhu, J. Chen, J. Duan, H. Liao, X. Zhu, Z. Li, I. McCulloch, W. Yue, *ACS Appl. Mater. Interfaces* **2022**, *14*, 43586.
- [47] S. Fratini, M. Nikolka, A. Salleo, G. Schweicher, H. Sirringhaus, *Nat. Mater.* **2020**, *19*, 491.
- [48] J. Yang, Z. Zhao, S. Wang, Y. Guo, Y. Liu, *Chem* **2018**, *4*, 2748.
- [49] S. L. Wu, Y. F. Huang, C. T. Hsieh, B. H. Lai, P. S. Tseng, J. T. Ou, S. T. Liao, S. Y. Chou, K. Y. Wu, C. L. Wang, *ACS Appl. Mater. Interfaces* **2017**, *9*, 14967.
- [50] F. C. Spano, *Acc. Chem. Res.* **2010**, *43*, 429.
- [51] M. Hecht, F. Wurthner, *Acc. Chem. Res.* **2021**, *54*, 642.
- [52] Q. Cao, J. Yang, T. Wang, Y. Li, X. Pu, J. Zhao, Y. Zhang, H. Zhou, X. Li, X. Li, *Energy Environ. Sci.* **2021**, *14*, 5406.
- [53] T. Lei, Z.-H. Guo, C. Zheng, Y. Cao, D. Liang, J. Pei, *Chem. Sci.* **2012**, *3*, 1162.
- [54] A. A. M. Yusof, M. A.-F. M. S. Januddi, K. M. Isa, M. N. Harun, *Int. J. Integr. Eng.* **2022**, *14*, 40.
- [55] S. Yunus, F. Spano, G. Patrinoiu, A. Bolognesi, C. Botta, D. Brühwiler, A. Z. Ruiz, G. Calzaferri, *Adv. Funct. Mater.* **2006**, *16*, 2213.
- [56] D. A. Bernards, G. G. Malliaras, *Adv. Funct. Mater.* **2007**, *17*, 3538.
- [57] D. Venkateshvaran, M. Nikolka, A. Sadhanala, V. Lemaur, M. Zelazny, M. Kepa, M. Hurhangee, A. J. Kronemeijer, V. Pecunia, I. Nasrallah, I. Romanov, K. Broch, I. McCulloch, D. Emin, Y. Olivier, J. Cornil, D. Beljonne, H. Sirringhaus, *Nature* **2014**, *515*, 384.
- [58] G. Y. Ge, J. T. Li, J. R. Wang, M. Xiong, X. Dong, Z. J. Li, J. L. Li, X. Y. Cao, T. Lei, J. L. Wang, *Adv. Funct. Mater.* **2021**, *32*, 2108289.